Reduced-order models for the seismic assessment of plan-irregular low-rise frame buildings

Article *in* Earthquake Engineering & Structural Dynamics · August 2022

DOI: 10.1002/eqe.3725

4 authors:

Sergio Ruggieri
Politecnico di Bari
31 PUBLICATIONS **320** CITATIONS
SEE PROFILE

Akrivi Chatzidaki
National Technical University of Athens
6 PUBLICATIONS **5** CITATIONS
SEE PROFILE

Dimitrios Vamvatsikos
National Technical University of Athens
210 PUBLICATIONS **8,267** CITATIONS
SEE PROFILE

Giuseppina Uva
Politecnico di Bari
132 PUBLICATIONS **1,743** CITATIONS
SEE PROFILE

REDUCED-ORDER MODELS FOR THE SEISMIC ASSESSMENT OF PLAN-IRREGULAR LOW-RISE FRAME BUILDINGS

Sergio Ruggieri[1*], Akrivi Chatzidaki[2], Dimitrios Vamvatsikos[2], Giuseppina Uva[1]

[1]Department DICATECh, Polytechnic University of Bari, Via Orabona, 4 – 70126, Italy

[2] Institute of Steel Structures, School of Civil Engineering, National Technical University, Heroon Polytechneiou 9157 80, Athens, Greece

[*]Correspondence: Sergio Ruggieri, e-mail: sergio.ruggieri@poliba.it

SUMMARY

A procedure is presented for deriving low-complexity structural models to predict the global response of asymmetric-plan low-rise frame buildings for purposes of class-level assessment. As a compromise between employing a full-scale multi-degree-of-freedom structural model versus an equivalent single-degree-of-freedom one, the challenge is to create an idealized 3D structure with few degrees-of-freedom that can match the inelastic response of a building for which full knowledge of geometrical and mechanical properties is available. Such a 3D reduced-order model can offset the computational cost related to performing multiple nonlinear dynamic analyses within the framework of Performance-Based Earthquake Engineering. To this goal, rules and equations are proposed for achieving equivalence among the linear and nonlinear properties (e.g., mass, stiffness, strength) of the building analysed and the related 3D reduced-order model. The procedure is applied on a sample of 15 existing reinforced-concrete frame school buildings, from the province of Foggia in Southern Italy, for which the full numerical models are available. Both calibrated and uncalibrated reduced-order models are created, exploring the limitations of the proposed order-reduction in a real-life case study.

KEYWORDS

Reduced-Order Models, Asymmetric-Plan Buildings, Class-Level Assessment, Fragility Functions, Seismic Performance

1. INTRODUCTION

Assessing the seismic behaviour and the related losses for a building portfolio is a crucial phase to devise risk reduction strategies and to address prioritizing interventions in earthquake-prone areas. To pursue this aim, several methodologies are available for determining seismic fragility and vulnerability. The path to follow depends on the quality and the quantity of available data for the building(s) in question, the desired numerical complexity, and accuracy of results, which drive the analyst to establish the type and number of analytical models to consider, the related modelling assumptions, and the analyses to perform. Generally, for deriving seismic fragility and vulnerability functions for any given class within a taxonomy, we have two different options for modelling archetype/index buildings[1], as shown in Figure 1: (a) a handful of multi-degree-of-freedom (MDOF) structures; (b) many single-degree-of-freedom (SDOF) oscillators; there are also two different options for analysis: (i) nonlinear static pushover analysis (SPO); (ii) nonlinear response history analysis (NRHA). On the analysis side, despite the evident computational frugality of the SPO, its results cannot easily account for the record-to-record variability, or features such as spectral shape, duration, etc., while NRHA can more accurately offer these, but its cost usually restricts its use to simpler models. On the modelling side, the adoption of many SDOFs provides a good coverage of the building stock, including different heights, vertical irregularities, code design levels etc. (Silva et al. [2]), but it fully misses local responses, as well as the detrimental effects of plan irregularities. A further improvement can be obtained if more complex 2D models are employed (e.g., see Sousa et al. [3]), together with correction factors, the so-called secondary modifiers, to approximately account for 3D features. At the high end, using a few 3D MDOFs (index buildings) can be a double-edged sword; while they offer sufficient accuracy on a building-by-building basis, they lack in coverage of a full class.

Optimally, one should run multiple NRHAs on numerous MDOFs with obvious computational issues. Instead, most practical applications resort to running NRHAs on many SDOFs or SPOs on few MDOFs. In the latter case, one could even try running a few NRHAs, hopefully strategically selected to deliver an adequate response estimate[4–6].

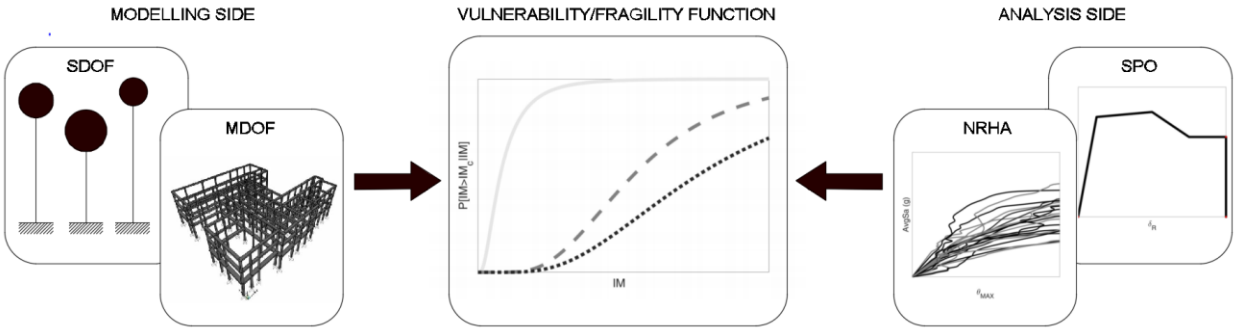

Figure 1 – Modelling/analysis options for deriving vulnerability/fragility functions

Otherwise, an honourable compromise between these two extremes is to reduce the complexity of the MDOFs, offering a reduced-order model that can capture the overall behaviour of the structure, delivering reasonable accuracy at an acceptable cost. Where class fragility is concerned, analysts have often resorted to *a priori* defining simplified archetypes, usually adopting symmetric-plan buildings without setbacks, and neglecting strength/mass/stiffness eccentricities or any other characteristic that would preclude the use of a 2D model. Going to a 3D model is by no means helpful for complexity reduction, especially given the myriads of ways one can deviate from regularity. The question at hand then, is whether a minimal mechanical model can be devised that can closely reproduce the salient dynamic characteristics of non-standardisable irregular-plan buildings. This latter approach is more attractive when a small group of actual structures rather than a set of idealized archetype index buildings is employed to characterize a class, lending higher realism, but also adding problems of model accuracy.
In this perspective, our aim is to provide a methodology to build idealized 3D reduced-order models that account for plan irregularities while having few degrees-of-freedom, able to simulate both elastic and inelastic structural response. The efficiency of our proposal is tested on a real class of reinforced concrete (RC) school frame buildings[4,7].

2. SIMPLIFIED MODELS IN SEISMIC PERFORMANCE ASSESSMENT

Simplified numerical models have often been adopted by the scientific community, aiming to achieve a compromise between accuracy of analysis and numerical complexity while still capturing the salient features of the full model. One can distinguish two types of such models, namely reduced-order and surrogate ones. Reduced-order models are mechanical models with a low number of degrees-of-freedom compared to the full model. Instead, surrogate models are essentially mathematical models, employing numerical functions fitted to a set of structural analysis results derived from the full model.
The simplest idea for a reduced-order model is naturally the SDOF system, which is the basis of the nonlinear static procedure[8,9]: An SDOF with a force-deformation backbone matching the pushover capacity curve of the MDOF structure is employed as a proxy for assessing global and local demands. A single-mass "joystick model" was proposed by Bakalis et al.[10] to capture the response of uplifting liquid-storage tanks in 3D. Still, for most building applications, 2D models are the norm, allowing us to capture the behaviour of a representative part of the building in a single vertical plane. A characteristic case is the "generic frame model" proposed by Nakashima et al.[11] for steel moment frames, comprising a representative column linked at each storey to a typical beam. A similar approach was adopted in the "fishbone models" [12–15], where beams are added on both sides of the column. The original concept is limited in terms of capturing the effect of overturning moments on column axial forces, restricting their applicability to relatively low-aspect ratio buildings. Newer fishbone models[16,17] have offered substantial improvements, but they are still constrained to 2D. A more recent example of a 2D reduced-order model is the "parsimonious model" proposed in Gidaris and Taflanidis[18]; this is a shear-structure model built using the results of cyclic pushover or sinusoidal dynamic analysis for calibrating the hysteretic behaviour. This was further improved by Patsialis and Tafalnidis[19] who offered an optimized framework for calibrating against NRHA results. Calibrated 3D stick models were also employed by Bovo and Savoia[20], using pushover analyses to derive the capacity curves of each storey and establish appropriate story-level properties of the simplified model, while d'Aragona et al.[21,22] proposed similar models for infilled RC buildings, using a database of existing structures to derive their properties. Recently, Blasone et al.[23] proposed a simplified 3D model having three DOFs per storey and using two translational springs per column. The seismic

behaviour of the building investigated is reproduced by a calibration process to also account for the flexibility and strength of the beams. To give some perspective, Lachanas and Vamvatsikos[24] explore the wide differences in computational time and associated error offered by several 2D and 3D simplified models for a single 20-story building. On the other end, surrogate models (e.g., Tsompanakis et al.[25], Taflanidis et al.[26]) are built exclusively on the premise of calibration, essentially fitting the results of the full model by means of meta-models that simulate as closely as possible the building response while being computationally cheaper. Such non-mechanical models establish a functional relation between the model parameters (input) and the model performance (output), for example by employing neural networks (Lagaros and Fragiadakis[27]), response surface models (Gavin and Yau[28], Taflanidis and Cheung[29]), or kriging models (Gidaris at al.[30], Gidaris and Taflanidis[31]). On one hand, this abstraction may create some issues of unidentifiability, where there is no physical connection to take advantage of engineering intuition for troubleshooting. At the same time, though, they offer some modelling flexibility, exploiting the implied continuity for the functional relation to allow the assessment of "interpolated structures", i.e., structures for which one has not created any physical model.

Overall, calibration seems to be an important part of employing reduced-order models, this being the case even for the equivalent SDOF system in a nonlinear static approach. Calibration can offer high accuracy, but it comes with a steep price: it requires creating and analysing the actual detailed model. Forming a full model is an onerous task, while achieving convergence in the nonlinear analysis of high-resolution models is costly, especially when considering realistic structures, rather than academic archetypes. Clearly, going straight to an acceptable reduced-order model, without needing a full one, is an advantage, especially when one seeks to capture the salient characteristics of the behaviour, rather than perform a detailed assessment.

With this goal in mind, we offer formal rules for transforming a low-rise asymmetric building to a facsimile 3D reduced-order model, capable of reproducing the salient dynamic characteristics of the original. The scope of this methodology is not to perfectly account for local failure mechanisms of individual components, but rather to capture an overall "average" behaviour (e.g., in terms of interstorey drift ratio, roof drift, top displacement) and allow, if needed, to improve upon this by adding calibration via a static pushover analysis. Whether this is a successful endeavour will typically depend on the characteristics of the building under investigation, as well as the desired degree of simplification.

3. THE TAVOLINO 3D REDUCED-ORDER MODEL

The proposed 3D reduced-order model is an idealized structure having the same number of storeys of the building investigated. It consists of one or more 3D rectangular-plan one-by-one bay idealized sub-structures (Figure 2), which can be termed "small tables", "mesillas", "tavolini" or "trapezakia", depending on one's linguistic preference. Herein, to honour the country of origin of the first author, the term tavolino will be employed (plural tavolini). These tavolini aim to reproduce both the elastic response of the building, by ensuring the equivalence of mass and stiffness, and the inelastic response, by considering the nonlinear features of all structural elements. Nevertheless, it is not strictly necessary for all building information to be available. For example, a tavolino model can be generated for an existing building, even if only historical documentation is available, e.g., original drawings, technical reports. Also, a simulated design process for a structure belonging to a certain building typology can provide all the necessary information. Once the in-plan shape of the original building is known, the analyst can define the number of tavolini to employ. Obviously, for the sake of simplicity, a building having a likely regular plan shape can be reproduced by a single tavolino, while strongly in-plan irregular buildings can be simulated by more than one tavolino. In this latter case, it is possible to identify roughly symmetrical parts of an otherwise asymmetric building, model each of them as one tavolino and join them via a rigid diaphragm to capture the entire structure. This breakdown and joining of the symmetric tavolini will offer the asymmetry representation, thus we strive to make the rules of tavolino creation as simple and transparent as possible to avoid unnecessary complications. From the analytical point of view, the method aims to reduce the mass and stiffness matrices size, while maintaining an imperfect but close-enough matching of the elastic properties. A perfect reproduction of the original building properties by the tavolino can only be achieved in the case of a perfectly regular structure, while some differences can be obtained in presence of irregularity sources, typical of existing buildings (e.g., misaligned columns, irregular in-plan distribution of beams and columns, etc.). In these cases, the results will be obviously suboptimal, yet easily upgradeable by a calibration process wherever a full model is available for the original building. More complex condensation rules can also be employed to improve the accuracy of the model a priori (e.g., albeit with a different aim, Priestley et al.[32] provide a weighted average approach to condense yield drift

of beams with different length, which could be easily integrated in the proposed simplified model). The analytical procedure to generate a tavolino model can be generalized in the following rules, which allow reproducing both elastic and post-elastic properties of the original building. The proposed procedure is herein developed and applied to low-rise RC structures but it can be extended to other frame building typologies (e.g., steel, wood), by means of adequate arrangements for the definition of the elastic and inelastic properties of structural elements. Nevertheless, further developments are required for wall structures (e.g., masonry).

Figure 2 – Concept of 3D reduced-order model by means of a two-story tavolino structure, applied on the B10 case study building (see also Fig. 5).

3.1 GEOMETRY AND ELASTIC PROPERTIES OF TAVOLINO MODEL

Let us assume that beams are arranged in the two principal directions, where the geometric features of the i^{th} element in the j^{th} principal direction are the cross-sectional area $A_{i,j}$, and the moments of inertia, $I^w_{i,j}$ and $I^v_{i,j}$, around the *w* and *v* local axes parallel to the width and height of the section, respectively. Subscripts "b" and "c" are used where needed to denote beams and columns, respectively. The geometric properties of each section will be used for performing the reduction, which is carried out per direction and it is characterized by different procedures for beams and columns. The N_b beams of each storey that span in the j^{th} principal direction are condensed into two identical parallel beams of the same direction in the tavolino, whose area, $A_{b,j}$, and inertia moments $I^w_{b,j}$, $I^v_{b,j}$ are computed as:

$$A_{b,j} = \frac{\sum_{i=1}^{N_{b,j}} A_{b,i,j}}{2} \tag{1}$$

$$I^w_{b,j} = \frac{\sum_{i=1}^{N_{b,j}} I^w_{b,i,j}}{2} \tag{2}$$

$$I^v_{b,j} = \frac{\sum_{i=1}^{N_{b,j}} I^v_{b,i,j}}{2} \tag{3}$$

The length of the two tavolino beams in the j^{th} direction, $L_{b,j}$, is estimated by the sum of the individual beam lengths $L_{b,i,j}$ along *j*, weighted by their corresponding moments of inertia, $I^w_{b,i,j}$:

$$L_{b,j} = \frac{\sum_{i=1}^{N_{b,j}} \left(I^w_{b,i,j} \cdot L_{b,i,j} \right)}{\sum_{i=1}^{N_{b,j}} I^w_{b,i,j}} \tag{4}$$

This weighted sum is accurate enough for beams of similar spans and widths, as typical in many old buildings, but it will not be as good if wide differences are present. The N_c columns of each story are condensed into four identical tavolino columns, whose inertia characteristics are:

$$I^w_c = \frac{\sum_{i=1}^{N_c} I^w_{c,i}}{4} \tag{5}$$

$$I_c^v = \frac{\sum_{i=1}^{N_c} I_{c,i}^v}{4} \tag{6}$$

The area of columns cannot be computed as done for the beams, because the element condensation should preserve the global resisting moment to overturning. To account for this effect, Eq. (1) can be re-edited by adding the Steiner term, which is given by the product of the area of the i^{th} column, $A_{c,i}$, and the square of the horizontal distance, d_i, between the centre of the considered column and the centre of mass of the building:

$$A_c = \frac{\sum_{i=1}^{N_c} [A_{c,i} + (A_{c,i} \cdot d_i^2)]}{4} \tag{7}$$

The height of the columns is assumed to be equal to the inter-storey height. The tributary mass of each column, M_n, assigned to its top node, can be approximated by equally subdividing the story mass M_s, among the four nodes of the storey s of the tavolino model:

$$M_n = \frac{M_s}{4} \tag{8}$$

From a computational point of view, M_n represents a translational mass and is applied in the two main horizontal directions. Still, it will also incur rotational mass vis-à-vis the tavolino center of mass, and due to the reduction of overall diaphragm dimensions (see Figure 3), this will be much lower than the actual building rotational mass. Specifically, the latter is related to the building floor mass moment of inertia, J_s, which in turn depends on the floor inertia radius, $i_{r,s}$:

$$J_s = M_s \cdot i_{r,s}^2 \tag{9}$$

If the total dimensions of the actual building sides (or the sides of the rectangle that encloses the building investigated) in the two main directions are L_x and L_y, the value of $i_{r,s}$ is provided by:

$$i_{r,s} = \sqrt{\frac{L_x^2 + L_y^2}{12}} \tag{10}$$

Hence, the rotational mass assigned to the four nodes, $J_{r,n}$, at each story of the tavolino is provided as the difference between the J_s of the original structure and the floor mass inertia moment of the simplified model, subdivided among the 4 nodes of the storey:

$$J_{r,n} = \frac{J_s - M_s \cdot \left(\frac{L_{b,x}^2 + L_{b,y}^2}{12} \right)}{4} \tag{11}$$

where $L_{b,x}$ and $L_{b,y}$ are the lengths of the beams (or sides) of the tavolino, or $L_{b,j}$ for $j = x, y$, respectively. Note that by using the enveloping rectangle for the actual building, while also assuming the tavolino mass to be spread over its diaphragm, Eq. (11) will tend to somewhat overestimate the rotational mass, something that may need to be fixed, especially for strongly plan-asymmetric buildings. Eqs (1) to (11) account for all the elastic properties of a tavolino model. The corresponding prototype, henceforth indicated with *nTav*, where *n* is the number of tavolini that compose the simplified model, is shown in Figure 3. To finally summarize the condensing rules for reproducing the elastic properties of the original building in the tavolino model, Eqs. (1) – (3) provide the equivalence of area and inertia for beams in both main directions; Eq. (4) gives a reasonable way to compute the plan tavolino dimensions, weighing for each direction beam lengths through their moments of inertia; Eqs. (5) – (7) provide the equivalence of area and inertia for columns in both main directions, compensating the number of columns decrease with an additional term to save the global structural behaviour to horizontal actions; Eqs. (8) – (11) ensure the equivalence in terms of translational and rotational masses.

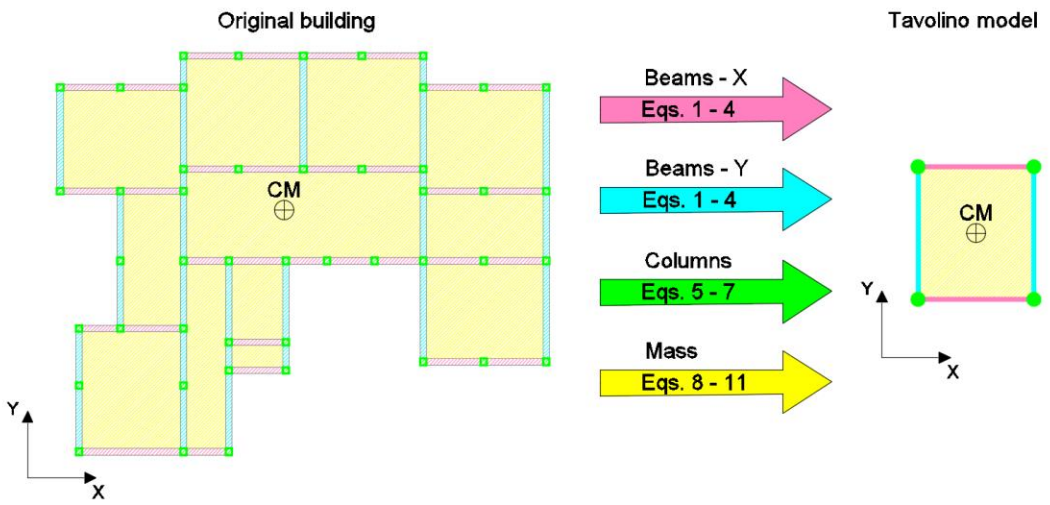

Figure 3 – Visual guide to make a 3D reduced-order model with 1*Tav* displayed in-plan, applied on case study building B10 (see Figure 4), only accounting for elastic properties. *CM* indicates the centre of storey mass.

It is apparent that, despite the consideration of the rotational mass of inertia, $J_{r,n}$, the 1*Tav* model will not be able to fully reproduce the coupled vibration modes of a strongly irregular building, because the centre of mass and the centre of stiffness coincide. Adding more tavolini to transition to *nTav* ideal structures, built from an *a priori* ideal subdivision of the real building in more parts, can offer this capability. In the latter case, the entire procedure is repeated *n* times, by incorporating in each replica all structural elements falling under the selected part of the building. An example of this concept is provided in Section 4, where each tavolino is positioned by ensuring correspondence with the centre of the mass of the considered real building part.

3.2 NONLINEAR BEHAVIOUR OF TAVOLINO MODEL

Concerning the nonlinear behaviour of the 3D reduced-order model, there are multiple paths one can follow, depending on the type of lateral-load system. For the case at hand, the simplest solution is a lumped plasticity model with plastic hinges located at the ends of the tavolino beams and columns. Simple nonlinear rotational springs are employed, without any axial-bending or biaxial-bending interaction. Each spring is characterized by a quadrilinear moment-rotation constitutive law, capturing (i) first cracking of concrete, (ii) yielding of the longitudinal bars with hardening behaviour, (iii) softening part for simulating the strength degradation of the section, (iv) residual moment assumed equal to 20% of the yielding moment (see Ruggieri et al.[7] for the graphical outline of the moment-rotation constitutive law). First, for each element of the actual building the values of the yielding, θ_y, and ultimate, θ_u, rotations are evaluated using the formula provided by Eurocode 8 – Part 3.3[33] (see also alternative expressions by O'Reilly and Sullivan[34]). The sum of the moment and of the rotation capacities of all beams acting in the j^{th} direction is split between the two tavolino j^{th} direction beams, while the corresponding sum of column capacities is divided by the four tavolino columns. Thus, the N_b beams of the actual building yield:

$$M_{by,j} = \frac{\sum_{i=1}^{N_b} M_{by,i,j}}{2}, \quad M_{bu,j} = \frac{\sum_{i=1}^{N_b} M_{bu,i,j}}{2} \tag{12}$$

$$\theta_{by,j} = \frac{\sum_{i=1}^{N_b} \theta_{by,i,j}}{N_b}, \quad \theta_{bu,j} = \frac{\sum_{i=1}^{N_b} \theta_{bu,i,j}}{N_b} \tag{13}$$

while, for the N_c columns we have:

$$M_{cy,j} = \frac{\sum_{i=1}^{N_c} M_{cy,i,j}}{4}, \quad M_{cu,j} = \frac{\sum_{i=1}^{N_c} M_{cu,i,j}}{4} \tag{14}$$

$$\theta_{cy,j} = \frac{\sum_{i=1}^{N_c} \theta_{cy,i,j}}{N_c}, \quad \theta_{cu,j} = \frac{\sum_{i=1}^{N_c} \theta_{cu,i,j}}{N_c} \tag{15}$$

where M_{by}, M_{bu}, M_{cy} and M_{cu} are the yielding (y) and ultimate (u) moments of beams (b) and columns (c), while θ_{by}, θ_{bu}, θ_{cy} and θ_{cu} are the yielding and ultimate rotations of beams and columns belonging to the reduced-order model.

Figure 4 shows a conceptual view of the nonlinear modelling for a 3D reduced-order model in the j^{th} direction, by employing a lumped plasticity approach and by showing the comparison with a full model. To account for shear failures in the tavolino model, the terms in the right hands of Eqs. (12) to (15) can be properly modified, by introducing the shear mechanism point in the moment-rotation constitutive law of beams and columns (e.g., Priestley et al.[32]).

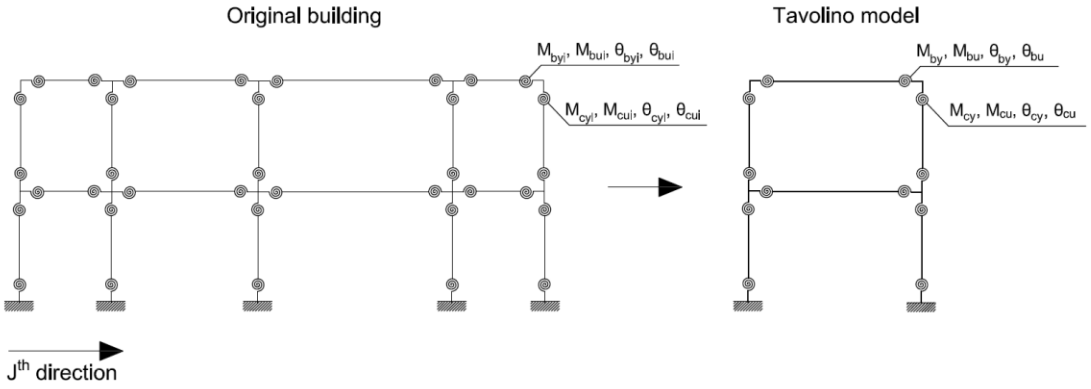

Figure 4 – Nonlinear modelling concept with 1*Tav* for the j^{th} direction, using a lumped plasticity approach.

4. CASE STUDIES

The proposed procedure has been tested on 15 existing RC school buildings, located in the Province of Foggia, Southern Italy. All buildings, labelled B1 to B15, are low-rise frame structures (2 or 3 storeys), built between the 1960s' and 1980s' only for gravity loads and with complex plan shapes[4,7].

Figure 5 shows the building plans and the corresponding 3D reduced-order models (in bold). For each building, the overall plan dimensions are reported, as well as the location of beams (lines) and columns (dots). Also, for the tavolini, the plan dimensions are indicated, as computed using Eq. (4). Figure 5 also reports the name of the municipality where each school is located. Specifically, Lesina (2) and Cerignola (2) refer to a second school complex within the municipality, composed of several independent structures: B6-B7-B8-B9 for Lesina (2); B11-B12-B13 for Cerignola (2). For buildings judged to be of low-to-moderate plan asymmetry, 1*Tav* models are employed. For the strongly plan-asymmetric B8, B12, B15, 2*Tav* models are preferred.

Observing Figure 5, some cases appear where the aspect ratio of the 1*Tav* model, i.e., the ratio of $L_{b,x}$ / $L_{b,y}$, differs from the aspect ratio of the original building, L_x / L_y. For example, for B5 the original building has the longer side in Y direction, while its tavolino has the longer side in X. This stems from the application of Eq. (4), where the value of $L_{b,j}$ is linked to the inertia of the cross sections of the beams, the length of each beam, and the number of beams acting in the j^{th} direction. The overall balance of these quantities plays a fundamental role in the definition of the plan shape of the simplified model.

For all buildings, full models are developed in SAP2000[35]. The tavolini are modelled using Opensees[36]. Beams and columns are modelled with lumped-plasticity elements, having plastic hinges characterized by an in-cycle degrading backbone and moderately pinching hysteresis without cyclic degradation. The effect of gravity loading has been accounted in the definition of column hinges, while the influence of infill panels has been neglected. Brittle failures due to insufficient transversal reinforcement or to the interaction between structure and masonry panels are evaluated in the post-processing phase.

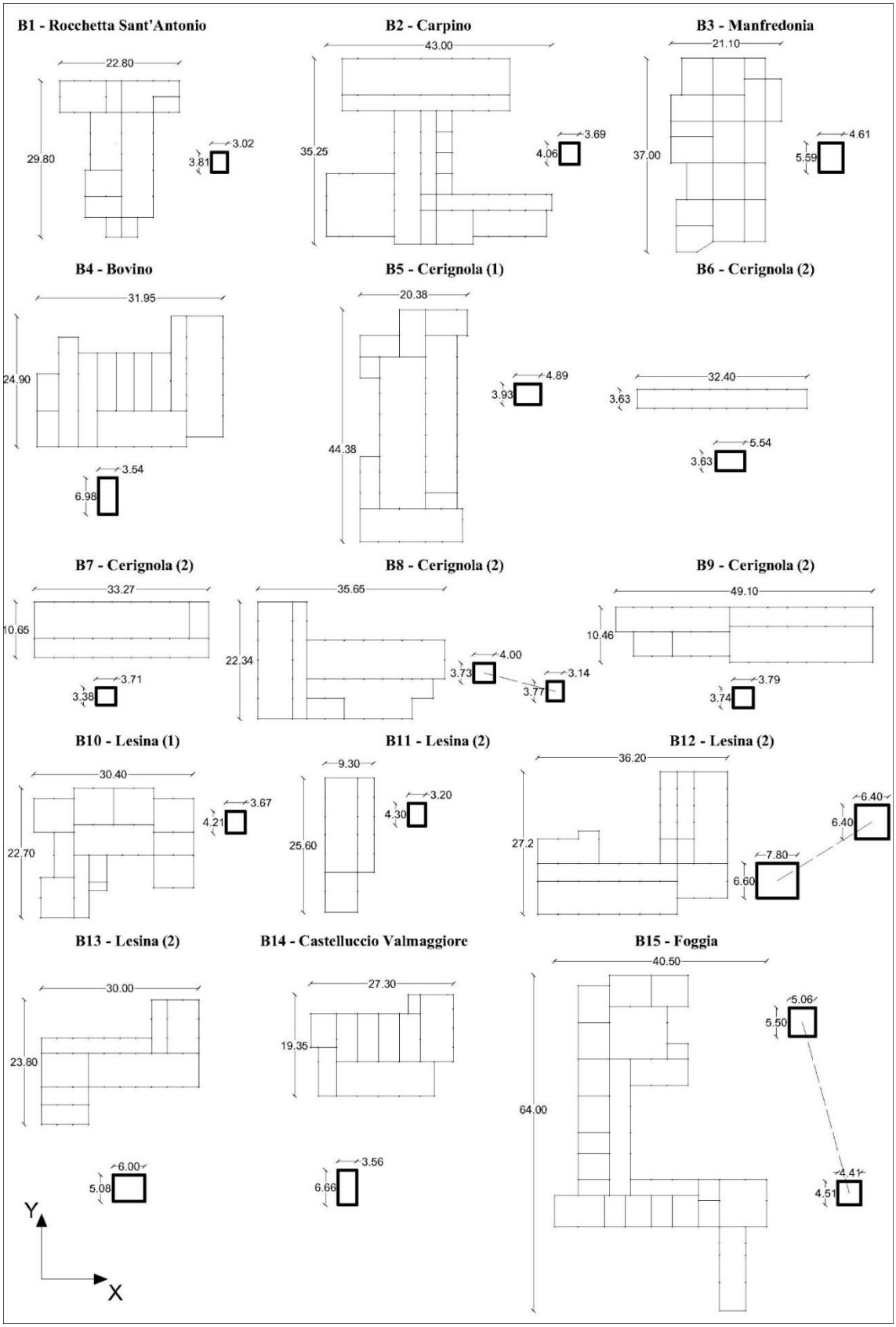

Figure 5 – Building plans and tavolino models for the 15 existing RC school buildings of Foggia, Italy.

For full models, three global limit-states are employed according to a composite-rules approach[4,37,38], namely immediate occupancy (IO), life safety (LS), and near collapse (NC). To this scope, the exceedance of the limit-states is not determined by the failure of any single element, as usually prescribed by current guidelines[33]. As a matter of fact, such strict interpretations of limit-states are almost always conservative and do not necessarily translate to the condition of the entire structure. Combined rules that explore the failure of more elements can offer a fair representation of overall building damage and loss, both for full and tavolino models. Then, IO is exceeded at an interstory drift of 0.5%. LS is violated if (1) 50% of all beams and columns reach a value of chord rotation equal to ¾ θ_u, (2) 50% of the columns of the first story reach ¾ θ_u (i.e., a soft story occurs), or (3) shear failure appears in any element. For NC violation: (1) any column reaches a value of chord rotation equal to θ_u, or (2) shear failure appears in any column. Using the results of SPO analysis, the engineering demand parameter (EDP) thresholds have been defined for the full models in terms of maximum interstorey drift, θ_{max}, in each principal direction. For reasons of simplicity, and to achieve a common basis for fragility comparison, these EDP values denoting failure of the full models have been also employed to denote failure of the tavolino models. In practice, one would expect adapting such rules for direct application to the tavolino models if no calibration to the full model is desired. For example, this can be achieved by establishing global criteria on the capacity curve (e.g., see Ricci et al.[39]).

To assess the accuracy of the tavolini, the first three periods (T_1, T_2, T_3) and the corresponding translational and rotational participating masses (M_X, M_Y, M_θ) are reported in Table 1. The periods obtained from full and 3D reduced-order models are comparable in all cases, which means that the numerical reduction accurately reproduces the full model elastic features. Some differences are obtained for 1*Tav* models that report higher participation mass values than the full models, due to imperfectly capturing the coupling of translational and rotational eigenmodes. For example, for building B2 the first X-translational (M_X = 46%) and rotational modes (M_θ = 47%) should be well-coupled due to the moderate plan asymmetry. Still, the 1*Tav* model is rectangular and plan-symmetric, thus unable to capture such a behaviour, reporting M_X = 96% and M_θ = 95%. If instead we subdivide the structure into four parts to better match its complex plan shape, we need to apply four times the steps of the proposed procedure to create each of the four tavolini and apply diaphragm constraints to reach the 4*Tav* model shown in Figure 6. Table 2 reports the corresponding eigenvalue results, showing a much higher degree of conformity for the 4*Tav*, both in terms of periods and participating masses (M_X = 67% and M_θ = 62%). On the other hand, this improvement comes with the cost of having a somewhat more complex model than 1*Tav*, but still a model that remains far simpler than the detailed full case. For simplicity, henceforth we only consider the simpler 1*Tav* or 2*Tav* versions for all case-studies, as presented in Figure 5, selectively showing 4*Tav* results for B2.

Table 1 – Comparison, in terms of periods and participating masses, between full and reduced-order models of the buildings (values for tavolini are reported in italic).

Building	No. storeys	Full models / *3D reduced-order models*					
		T_1 (s)	T_2 (s)	T_3 (s)	M_X (%)	M_Y (%)	M_θ (%)
B1	2	0.32 / *0.33*	0.31 / *0.32*	0.28 / *0.28*	79 / *93*	83 / *92*	84 / *94*
B2	3	0.84 / *0.78*	0.83 / *0.73*	0.73 / *0.67*	46 / *96*	91 / *91*	47 / *95*
B3	2	0.36 / *0.36*	0.32 / *0.34*	0.30 / *0.30*	90 / *89*	84 / *91*	85 / *91*
B4	3	0.83 / *0.85*	0.54 / *0.57*	0.51 / *0.50*	87 / *90*	62 / *71*	57 / *87*
B5	3	0.38 / *0.38*	0.30 / *0.33*	0.23 / *0.27*	77 / *75*	79 / *78*	78 / *81*
B6	2	0.52 / *0.52*	0.41 / *0.41*	0.34 / *0.31*	99 / *93*	86 / *93*	88 / *98*
B7	2	0.75 / *0.71*	0.59 / *0.35*	0.56 / *0.54*	53 / *98*	92 / *92*	51 / *98*
B8	2	0.74 / *0.80*	0.59 / *0.62*	0.58 / *0.60*	89 / *92*	61 / *67*	60 / *69*
B9	2	0.69 / *0.67*	0.67 / *0.62*	0.58 / *0.53*	99 / *98*	92 / *93*	94 / *99*
B10	2	0.43 / *0.43*	0.40 / *0.42*	0.39 / *0.38*	58 / *98*	71 / *98*	42 / *98*
B11	2	0.60 / *0.56*	0.45 / *0.47*	0.40 / *0.45*	91 / *93*	97 / *97*	94 / *97*
B12	2	0.54 / *0.53*	0.46 / *0.47*	0.43 / *0.44*	92 / *83*	50 / *61*	53 / *64*
B13	2	0.48 / *0.47*	0.41 / *0.41*	0.31 / *0.33*	69 / *95*	93 / *95*	70 / *97*
B14	3	0.79 / *0.83*	0.78 / *0.74*	0.66 / *0.71*	85 / *93*	75 / *90*	81 / *93*
B15	3	0.59 / *0.68*	0.57 / *0.65*	0.48 / *0.56*	84 / *87*	63 / *84*	61 / *88*

Table 2 – Comparison of periods and participating masses, among full, 1*Tav* and 4*Tav* models, for case B2.

Building B2	T_1 (s)	T_2 (s)	T_3 (s)	M_X (%)	M_Y (%)	M_0 (%)
Full model	0.84	0.83	0.73	46	91	47
1*Tav*	0.78	0.73	0.67	96	91	95
4*Tav*	0.83	0.76	0.71	67	91	62

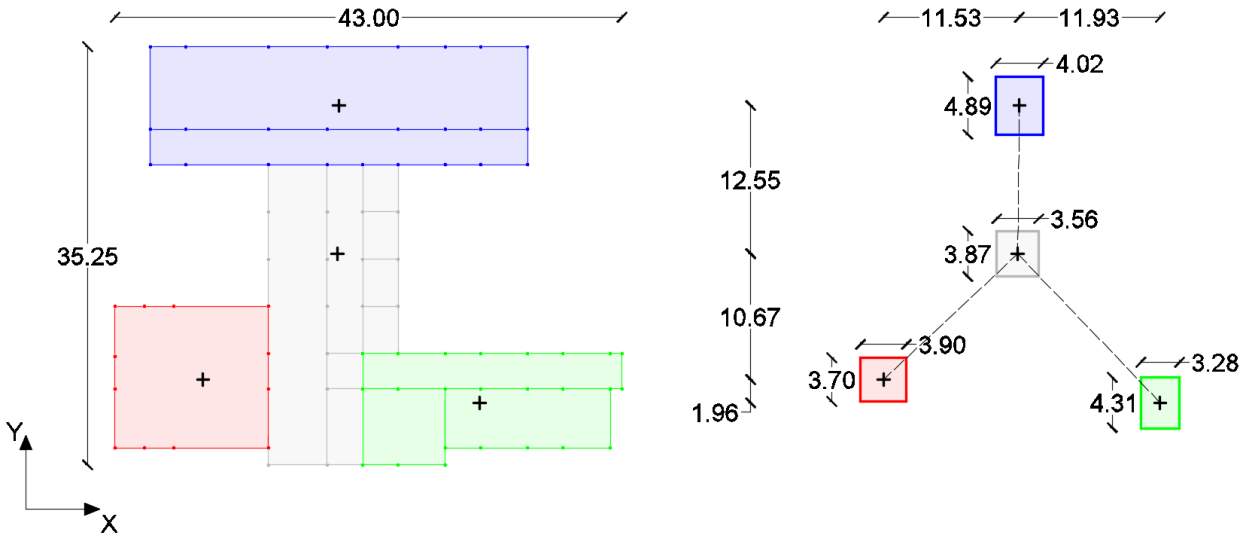

Figure 6 – Plan view of the B2 building (left) and corresponding 4*Tav* reduced-order model (right). The individual tavolini are placed so as to match the centre of mass of the corresponding building part, as highlighted by the crosses.

5. MODEL ASSESSMENT AND CALIBRATION

After the eigenvalue analysis, SPOs have been performed on the full and reduced-order models of all buildings investigated. All SPOs have been carried out in the two main directions X and Y, by applying a uniform load pattern on the centres of mass. Figures 7 and 8 show SPO results in terms of base shear, V_b, versus roof displacement, δ_R. Comparing the capacity curves of the full (blue continuous lines) and the 3D reduced-order models (black dashed lines), it can be observed that for all buildings and directions, the slopes of the initial elastic branches almost always coincide, due to an effective reproduction of the elastic parameters by the tavolini. Going from the yielding values of capacity curves to the hardening and softening branches, the results show some differences in terms of slope and ductility. This effect can be attributed to the nature of the 3D reduced-order model, which cannot take into account the continuous stiffness variations of each structural element of the full models in the post-elastic range; it can only predict the global trend of building behaviour. These discrepancies do not allow a perfect capturing of the nonlinear structural response by the tavolino in its uncalibrated version.

As an improvement, a calibration of the original tavolino models has been carried out, by modifying some of their parameters to match the SPO response of the full models in both main directions. Specifically, only parameters of the constitutive laws employed in plastic hinges have been modified, such as the values of yielding moments, hardening and softening slopes of post-elastic branches and ductility ratios. This step has been performed by opting for an iterative calibration of the above parameters for all plastic hinges of the tavolino, until obtaining a near-perfect superposition of the reduced-order model capacity curves to those provided by the full model. Hence, the results of SPO performed on the modified version of the tavolini models, here indicated as calibrated, are reported in Figures 7 and 8 (black dotted lines) for B5, B8 and B10, where the capacity curves of calibrated models show a reliable reproduction of the full model trends, both in the elastic and post-elastic branches. Given the inherent cost of calibration, one may instead opt for increasing the complexity of the (uncalibrated) tavolino. Figure 9 shows SPO results for the uncalibrated 4*Tav* and 1*Tav* models of B2, where the more complex model better captures the global response without needing any help from the analysis of the full model.

Having the SPO results for the full models and the calibrated/uncalibrated tavolini, our proposal needs to be assessed by considering their NRHA results. To this scope, we use the same set of 11 natural ground motions employed in Ruggieri et al.[4] (see Section 6), extracted from the moderate seismicity sample of records provided by the INNOSEIS project[40]. This is a subset of the 30 ground motion records proposed in the abovementioned project, selected through the Conditional Spectrum approach[41,42] to be compatible to the hazard with 2% probability of exceedance in 50 years for some European moderate seismicity sites. The adopted set of records, herein labelled E1 to E11, are considered a fair representation of the region of Foggia with peak ground acceleration values around 0.20 – 0.25g.

As an example, the results of NRHA for five buildings and five accelerograms are shown in Figures 10 and 11, reporting the absolute normalized difference between the full and the reduced models in the two main directions of θ_{max} and δ_R for the calibrated and uncalibrated models. In some cases, fewer than five records are shown due to numerical convergence issues encountered with the analyses of the full models. The differences are in the order of 5% to 20% for most cases, with a sole exception reaching 30%. Differences recorded for the calibrated models are only mildly lower than the ones for uncalibrated models, and in some cases negligible. This latter comparison indicates that the proposed 3D reduced-order model can be employed for assessing the seismic response of the buildings, without necessarily requiring calibration, especially if ensemble assessment is the target.

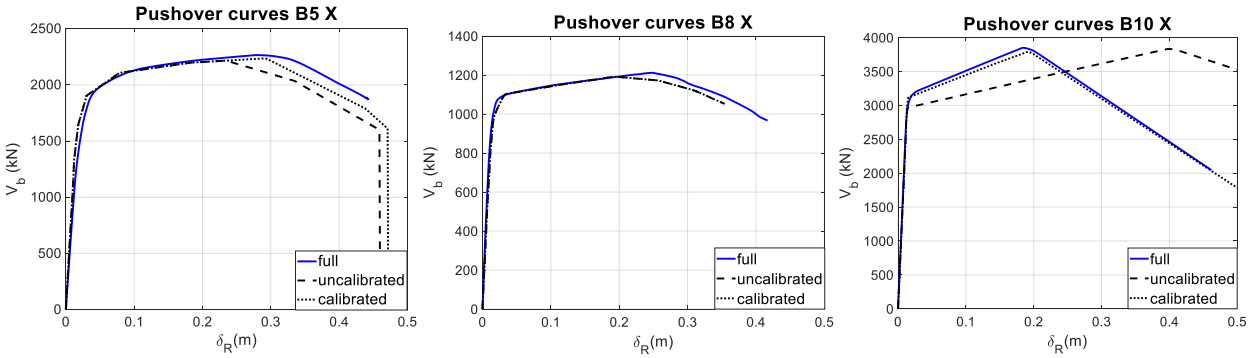

Figure 7 – Pushover curves of the full, calibrated and uncalibrated 3D reduced-order models for B5, B8 and B10, X direction.

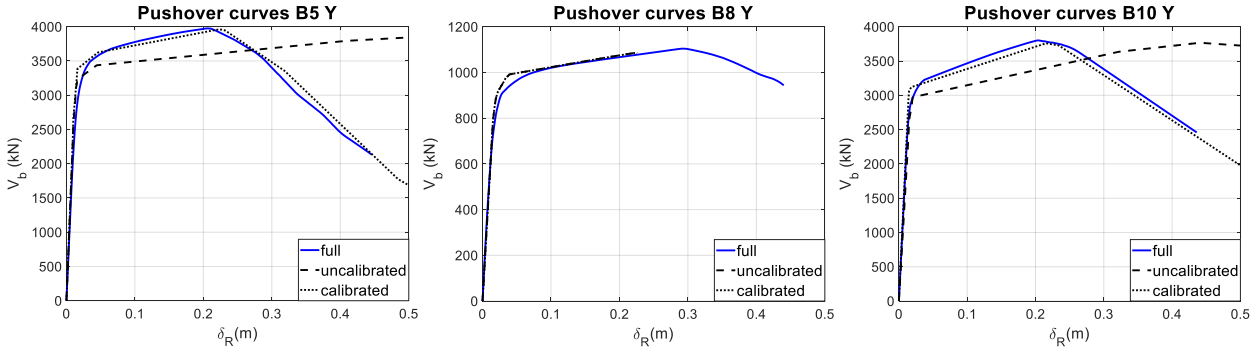

Figure 8 – Pushover curves of the full, calibrated and uncalibrated 3D reduced-order models for B5, B8 and B10, Y direction.

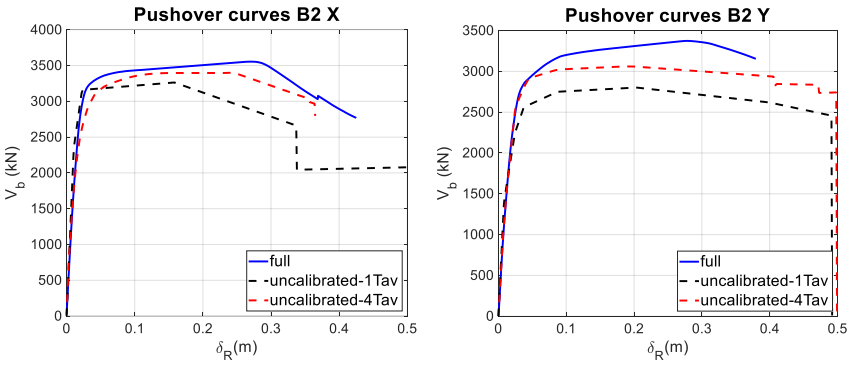

Figure 9 – Pushover curves of the full, and uncalibrated 1*Tav* and 4*Tav* reduced-order models for B2, X and Y directions.

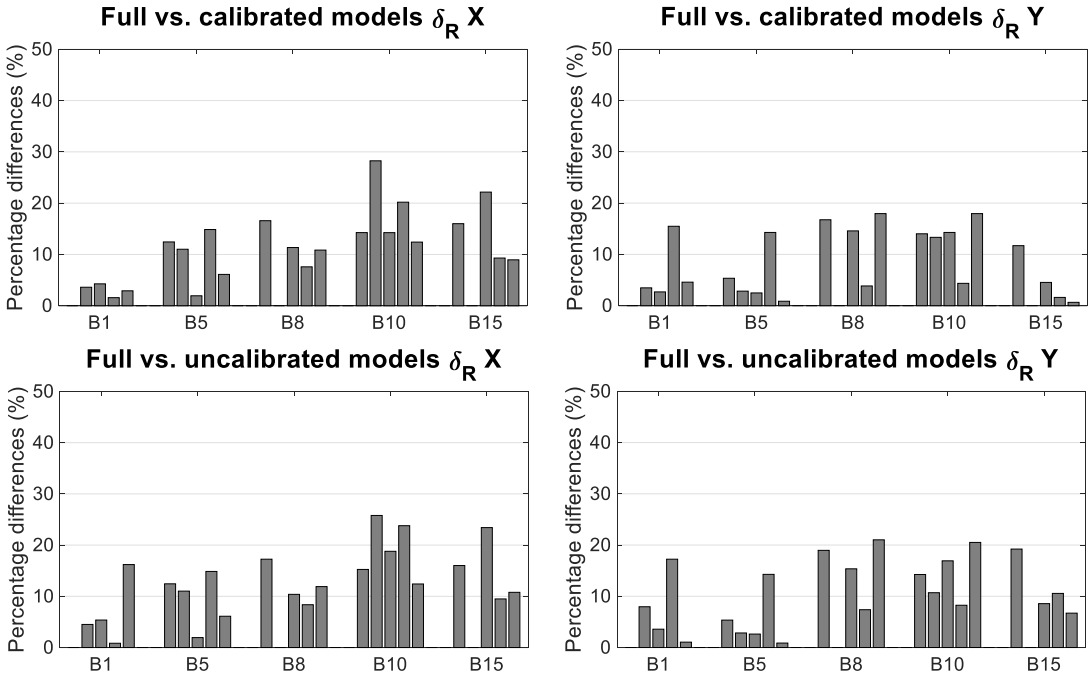

Figure 10 – Percentage differences of the peak roof displacement δ_R between the full versus the calibrated (top), and the uncalibrated (bottom) tavolini, in the two main directions. Results are shown for five buildings and five ground motion records each.

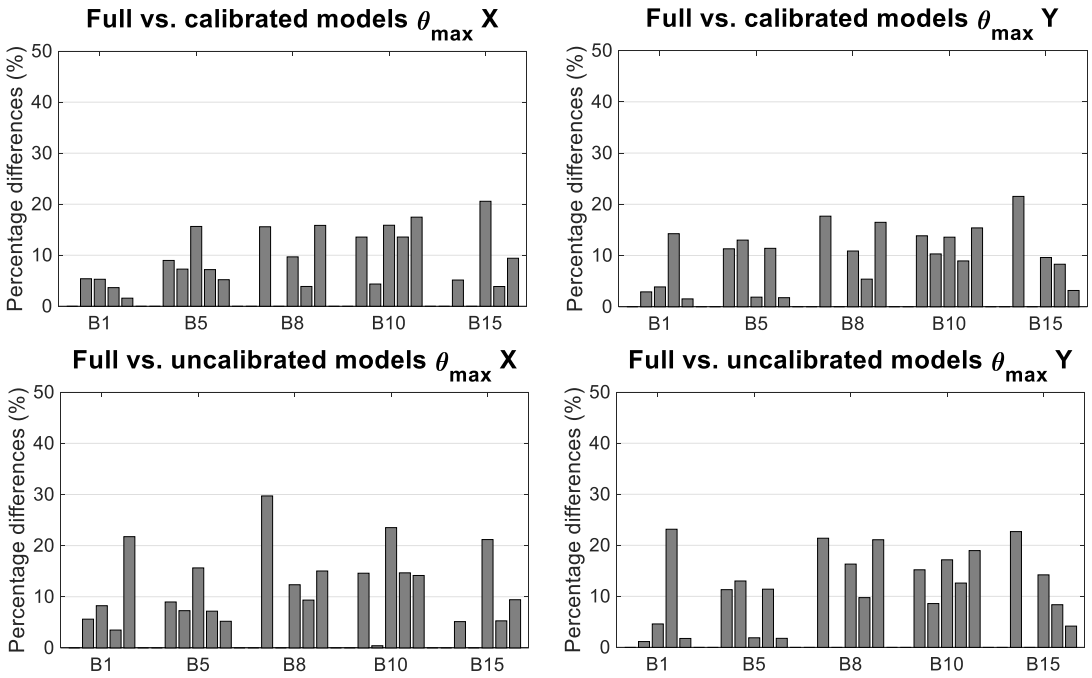

Figure 11 – Percentage differences of the maximum interstorey drift ratio θ_{max} between the full versus the calibrated (top), and the uncalibrated (bottom) tavolini, in the two main directions. Results are shown for five buildings and five ground motion records each.

6. FRAGILITY ASSESSMENT

The SPO and NRHA performed in Section 5 have shown the ability of the proposed 3D reduced-order models to predict the static and dynamic structural response of the full models, even without calibration. To assess the structural response for the different modelling approaches, a more intensive NRHA assessment is necessary. It is worth remembering that the proposed procedure is meant to benefit the analyst by offering a compromise between (i) the detailed assessment of a few detailed MDOFs, for which the right choice of significant properties can be problematic, and (ii) the simplified assessment of many SDOFs, which cannot account for secondary characteristics, especially plan-irregularity. NRHA is the method of choice for the tavolini, which combined with a moderate number of records can offer the needed middle ground. Herein, we use the abovementioned set of 11 ground motion records, a number that conforms with ASCE7-16[43]. As the EDP we employ the square-root-sum-of-squares (SRSS) of the θ_{max} values recorded in the two main directions, which is a comparable parameter between full and 3D reduced-order models, and it can be well identified with the employed number of records[4]. Finally, we adopt as intensity measure (IM) the average spectral acceleration (*AvgSa*[44]) in a period range of 0.2 s – 2.0 s with an increment of 0.1 s; this can well represent the behaviour of low/mid-rise buildings governed by three main vibration modes (two translational, one rotational).

To perform a full range estimation via NRHA, several methods can be adopted, such as incremental dynamic analysis (IDA[45]), cloud analysis[46] or multi stripe analysis (MSA[47]). Their application on full models can become computationally prohibitive, but it is a relatively painless business for the tavolini. Herein, the tavolini models (both calibrated and uncalibrated) have been subjected to IDAs, while the full models have been subjected to a simplified version of MSA, the few stripe analysis (FSA)[4], which consists of running three stripes: the first is performed at a fixed intensity value selected based on the elastic code spectrum, while the second and the third are sequentially defined by appropriately increasing or decreasing the intensity value given the appearance of collapse/non-collapse in earlier runs. FSA was employed in Ruggieri et al.[4] on the same set of buildings, using the geometric mean of the spectral acceleration values for the first three main periods of vibration ($AvgSa_3$) as the IM. The results have been readapted to match the IM of *AvgSa* employed here, using the ratio of *AvgSa* over $AvgSa_3$, evaluated on a record-by-record basis. Thus, changing the IM, turns the three stripes into a small cloud. A sample of results is presented in Figure 12 for B5, B8 and B10, where IDA curves for uncalibrated tavolini are shown along with the FSA points for the full models. Similar results were obtained by performing IDAs on the calibrated tavolini, not shown here for the

sake of brevity. For cloud analysis, the non-collapsed points are displayed in black, while the collapsed points are depicted in red and placed at the far right of each graph. The comparison between the two modelling and analysis approaches reveals differences depending on the IM level. At the near-elastic range of low *AvgSa* values, the cloud points overlap nicely with the IDA curves. Moving to higher values of IM, it can be more difficult to achieve a fair comparison as the appearance of collapsing starts to become an issue. Given the low number of records and the few overall runs used in FSA, every collapse removes one visible point, making it difficult to compare. For sure, though, the full model of building B5 does seem to collapse earlier than its corresponding tavolino, while B8 and B10 are better captured.

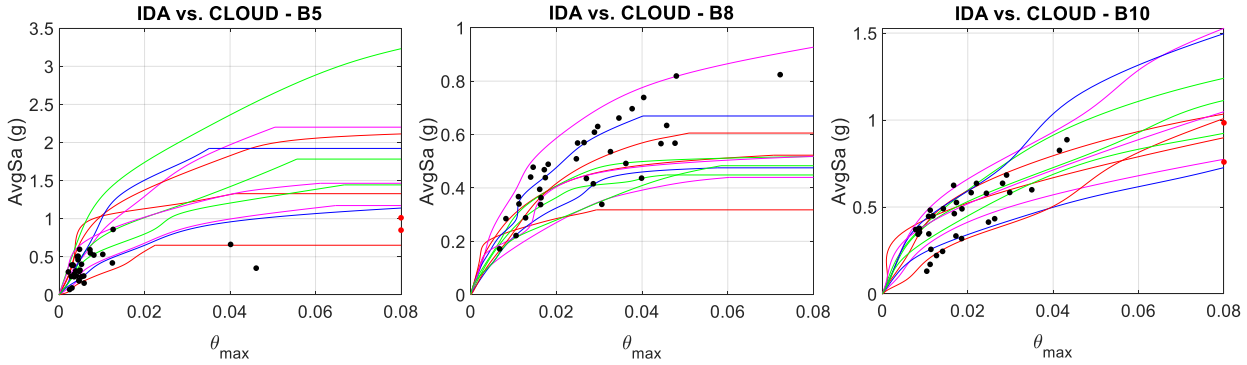

Figure 12 – Incremental dynamic analysis, IDA, results of the uncalibrated 3D reduced-order model vs. cloud analysis results of the full models, for B5, B8 and B10, in terms of average spectral acceleration, *AvgSa*, and maximum interstorey drift ratio, θ_{max} SRSS combination. The no collapse points obtained in the cloud analysis are presented in black while the collapse ones are shown in red colour at the right edge of each graph.

For a more careful comparison we now turn to fragility. Fragility curves provide the probability of violating a limit-state, associated to a certain EDP threshold, EDP_{lim}, formalized as $P[EDP > EDP_{lim} \mid IM]$[48]. They are typically represented by lognormal distributions, characterized by the median value, μ, and the associated dispersion, β. Several options can be pursued for computing fragility curves, on the basis of the analysis method employed. Herein, the fragility curves of the reduced-order models are computed by employing "vertical statistics", as originally termed by Krawinkler[49], i.e., IM-basis estimation of structural response given a value of EDP. For the FSA results of the full models, the power-law approximation proposed by Cornell et al.[44] is adopted to obtain a continuous representation of the IM-EDP response, which is used as a basis for computing the fragility curves. As discussed in Section 4, the limit-states of IO, LS and NC are defined separately under the assumption of ductile or brittle mechanisms, using θ_{max}. To quantify the total variability, an additional 30% dispersion was incorporated via an SRSS rule for all limit-states, originally stipulated in FEMA P-695[50] for NC.

Figure 13 shows a sample of results obtained for B4 and B5 as examples of optimal and suboptimal fragility estimates, respectively. Three graphs are presented for each building, one per each of the three limit-states and considering ductile versus brittle mechanisms for the limit-states. In each graph, three fragility curves are reported, corresponding to the full (continuous line), uncalibrated tavolino (dashed line) and calibrated tavolino (dotted line) models. The differences between the calibrated and uncalibrated tavolini are negligible, showing similar fragility curves with small discrepancies in terms of μ and, in most cases, they are nearly coincident. This result confirms that the proposed procedure provides reduced-order models that do not necessarily require calibration. Juxtaposing the results of the full and the reduced-order models, several observations can be traced. Referring to the fragility curves for IO the results are very close in absolute value but in terms of percentage differences with the full models the trend is discontinue. As a matter of fact, for models B4, B5, B6, B8, B10 and B13 the percentage differences of μ and β range from 10 to 30%, thus confirming that the tavolini can capture the elastic and the near-yielding behaviours of full models. Going to models B3, B11 and B14, the percentage differences increase around values of 50-70%. Higher differences are obtained for models B1, B2, B7, B12 and B15, achieving percentage differences of more than 100%. Same conclusions can be drawn for brittle mechanisms at LS and NC limit-states. The observed high differences in some cases are due to a number of reasons, e.g., different analysis method, use of few records, choice of the minimum number of tavolini per building. Despite the varying results, this is a valuable achievement for more than half of the cases, especially for

older RC buildings presenting low-ductile behaviour in the near-yield range with occurrence of shear mechanisms at lower displacements, as for the sample of buildings investigated. When considering LS and NC for ductile mechanisms, the results somewhat deteriorate in absolute value, but looking at the results in terms of percentage differences of μ and β, a better picture is obtained. For models B1, B3, B5, B6, B8 and B9, percentage differences range from 30 and 40%, while for the remaining models the limit of 20% is not exceeded.

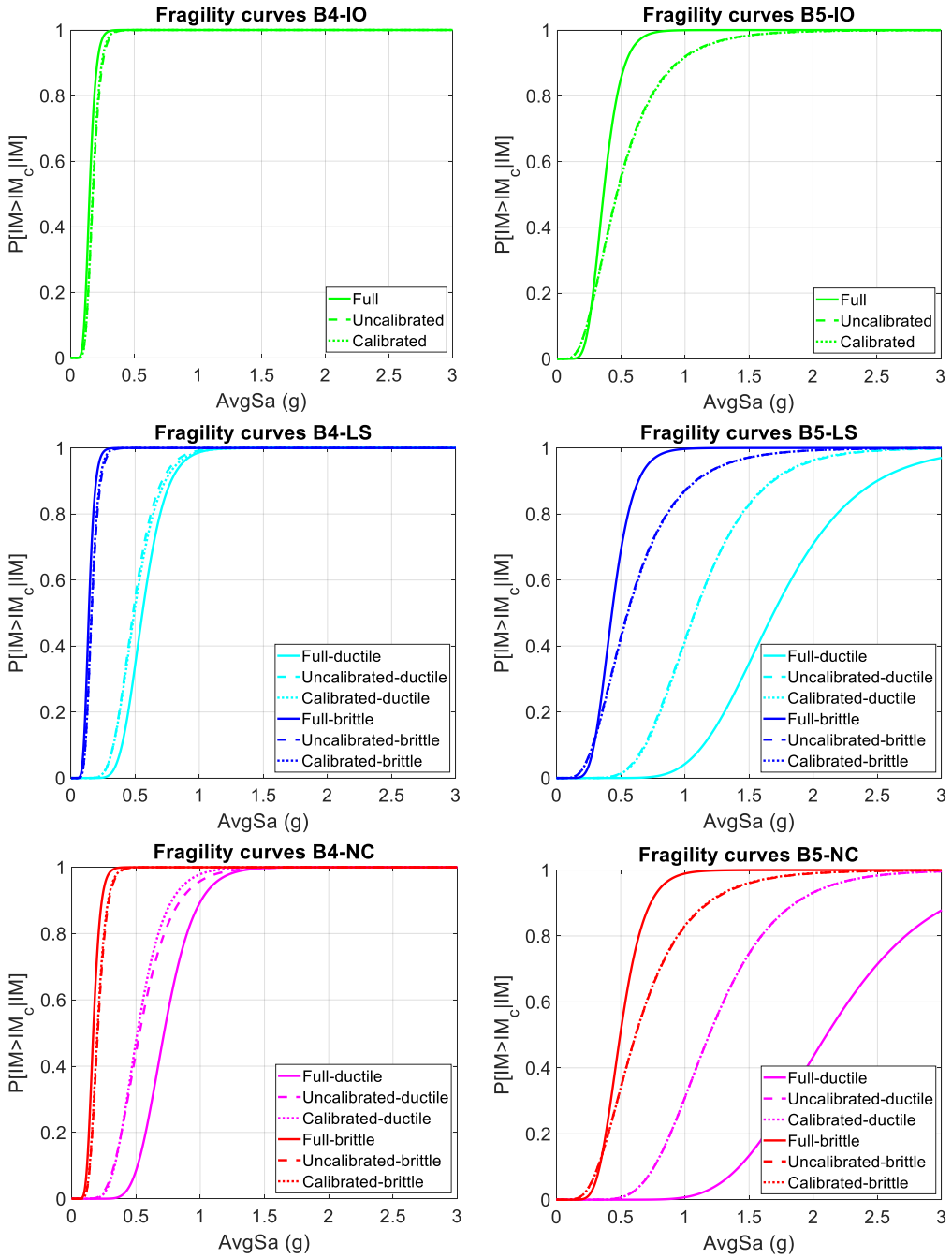

Figure 13 – Comparison of the fragility curves for B4 and B5 buildings, considering full, calibrated and uncalibrated models, failure mechanisms and limit-states.

Considering the case of B5, the fragility curves of the tavolini present slightly non-conservative estimates for low capacity EDP values (IO and brittle LS and NC) and conservative estimates for high capacity EDP values (ductile LS

and NC). In order to underline the advantages of tavolino, an additional comparison is introduced by employing simple SDOF models. For both main directions, the pushover curves of the full models are employed to define elastoplastic SDOF systems in Opensees. IDAs were run through the same set of records employed for other models and the weaker direction is considered for the sake of comparison. Results in Table 3 show that SDOF models provide always lower values in terms of μ than full and tavolini models, introducing considerable bias due to their limitations in accounting for three-dimensional effects (e.g., torsion). While one would expect the absence of torsion to work in favor of the SDOFs, rather than against, there is a number of approximations at play here that can shift the result one way or another, SDOF fragility curves are evaluated on the weaker direction of full models, while the comparison between SDOF and MDOF fragility curves is ruled by the degree of modelling simplicity and analysis accuracy[51]. In the end, of interest in this study is not which is the model that first exceeds a certain limit-state, but the "distance" from the full model to the simplified ones (e.g., tavolino and SDOF). Table 3 reports μ and β values for all buildings, limit-states and modelling approaches. Considering the reduced number of records involved and the approximations in employing FSA on full models, the overall balance is positive. The tavolini provide results not far from the full models (especially for elastic or near-yielding ranges) with low computational costs and the capability of full investigation of elastic and inelastic building response via intensive IDA/MSA methods and, above all, without requiring a calibration process. In addition, as a goal initially set, the proposed reduced-order model is capable of reproducing to a fair extent the effect of plan irregularities of the buildings investigated, which is not of SDOF models competence. Nevertheless, the results suggest that 1-2*Tav* models may encounter a certain loss of accuracy for building-specific investigations when complex plan shapes are involved.

Table 3 – μ and β values of fragility curves, accounting for all limit-states (IO, LS and NC), all modelling approaches (full, calibrated, uncalibrated and SDOF), and all collapse mechanisms considered (ductile and brittle).

Building	Model	IO		LS (Ductile)		NC (Ductile)		LS (Brittle)		NC (Brittle)	
		μ	β	μ	β	μ	β	μ	β	μ	β
B1	Full	0.098	0.32	0.941	0.32	1.223	0.32	0.041	0.33	0.085	0.32
	Calibrated	0.234	0.42	0.657	0.24	0.682	0.25	0.111	0.51	0.210	0.44
	Uncalibrated	0.284	0.38	0.716	0.26	0.761	0.26	0.169	0.55	0.260	0.41
	SDOF	0.065	0.57	0.470	0.32	0.558	0.31	0.027	0.57	0.056	0.58
B2	Full	0.090	0.29	0.446	0.29	0.596	0.29	0.057	0.30	0.098	0.29
	Calibrated	0.192	0.18	0.556	0.21	0.594	0.21	0.130	0.21	0.205	0.18
	Uncalibrated	0.200	0.29	0.512	0.22	0.550	0.22	0.137	0.29	0.207	0.29
	SDOF	0.028	0.32	0.161	0.33	0.232	0.33	0.017	0.32	0.031	0.32
B3	Full	0.192	0.35	1.740	0.35	2.246	0.35	0.082	0.36	0.110	0.35
	Calibrated	0.330	0.57	0.976	0.22	1.062	0.22	0.154	0.49	0.211	0.49
	Uncalibrated	0.322	0.52	0.960	0.22	1.050	0.22	0.153	0.49	0.212	0.48
	SDOF	0.077	0.54	0.489	0.52	0.491	0.50	0.037	0.54	0.048	0.54
B4	Full	0.149	0.27	0.557	0.26	0.718	0.26	0.139	0.27	0.167	0.27
	Calibrated	0.176	0.28	0.484	0.30	0.528	0.37	0.161	0.29	0.202	0.28
	Uncalibrated	0.173	0.27	0.493	0.31	0.510	0.33	0.159	0.27	0.199	0.28
	SDOF	0.028	0.32	0.122	0.32	0.172	0.33	0.026	0.32	0.032	0.32
B5	Full	0.363	0.31	1.690	0.31	2.103	0.31	0.431	0.31	0.496	0.31
	Calibrated	0.465	0.55	1.075	0.35	1.189	0.35	0.551	0.53	0.617	0.51
	Uncalibrated	0.468	0.55	1.078	0.35	1.189	0.35	0.555	0.52	0.617	0.50
	SDOF	0.056	0.45	0.257	0.46	0.308	0.47	0.066	0.45	0.076	0.45
B6	Full	0.214	0.31	1.659	0.31	1.847	0.31	0.235	0.31	0.277	0.31
	Calibrated	0.274	0.44	1.068	0.23	1.100	0.23	0.302	0.44	0.368	0.43
	Uncalibrated	0.263	0.44	1.039	0.24	1.069	0.25	0.289	0.44	0.359	0.42
	SDOF	0.039	0.40	0.309	0.33	0.342	0.31	0.043	0.40	0.051	0.40
B7	Full	0.053	0.43	0.464	0.43	0.835	0.43	0.062	0.43	0.074	0.43
	Calibrated	0.194	0.21	0.444	0.25	0.447	0.29	0.208	0.20	0.223	0.19
	Uncalibrated	0.189	0.18	0.429	0.24	0.443	0.28	0.208	0.18	0.223	0.18
	SDOF	0.028	0.32	0.133	0.32	0.193	0.31	0.031	0.32	0.036	0.32
B8	Full	0.168	0.22	0.492	0.22	0.730	0.22	0.163	0.22	0.173	0.22
	Calibrated	0.154	0.26	0.424	0.24	0.479	0.25	0.149	0.26	0.159	0.25
	Uncalibrated	0.154	0.26	0.424	0.24	0.479	0.25	0.149	0.26	0.159	0.25

	SDOF	0.028	0.32	0.120	0.29	0.213	0.32	0.027	0.32	0.029	0.32
B9	Full	0.067	0.36	0.418	0.36	0.702	0.36	0.064	0.36	0.071	0.36
	Calibrated	0.164	0.25	0.423	0.24	0.451	0.21	0.159	0.25	0.169	0.25
	Uncalibrated	0.164	0.25	0.423	0.24	0.451	0.21	0.159	0.25	0.169	0.25
	SDOF	0.027	0.32	0.135	0.33	0.210	0.32	0.026	0.32	0.258	0.32
B10	Full	0.163	0.25	0.723	0.25	0.855	0.25	0.141	0.25	0.174	0.25
	Calibrated	0.249	0.50	0.686	0.25	0.754	0.24	0.211	0.48	0.267	0.49
	Uncalibrated	0.254	0.46	0.632	0.23	0.699	0.24	0.219	0.49	0.270	0.44
	SDOF	0.051	0.48	0.333	0.48	0.407	0.39	0.043	0.48	0.055	0.48
B11	Full	0.102	0.31	0.770	0.31	0.957	0.31	0.102	0.31	0.111	0.31
	Calibrated	0.167	0.35	0.749	0.28	0.795	0.28	0.167	0.35	0.175	0.35
	Uncalibrated	0.182	0.34	0.747	0.28	0.783	0.28	0.182	0.34	0.188	0.34
	SDOF	0.038	0.38	0.260	0.31	0.316	0.32	0.038	0.38	0.042	0.39
B12	Full	0.103	0.31	0.694	0.31	0.889	0.31	0.108	0.31	0.112	0.31
	Calibrated	0.282	0.35	0.701	0.22	0.741	0.22	0.291	0.34	0.298	0.34
	Uncalibrated	0.271	0.35	0.714	0.22	0.795	0.22	0.281	0.34	0.289	0.33
	SDOF	0.042	0.42	0.284	0.31	0.326	0.30	0.044	0.42	0.046	0.42
B13	Full	0.201	0.21	0.713	0.21	0.917	0.21	0.205	0.21	0.227	0.21
	Calibrated	0.259	0.35	0.712	0.18	0.765	0.19	0.264	0.35	0.295	0.33
	Uncalibrated	0.261	0.35	0.711	0.18	0.765	0.19	0.266	0.35	0.297	0.33
	SDOF	0.046	0.47	0.256	0.32	0.324	0.30	0.047	0.47	0.054	0.48
B14	Full	0.098	0.32	0.486	0.32	0.643	0.32	0.041	0.34	0.061	0.33
	Calibrated	0.174	0.24	0.527	0.26	0.596	0.26	0.081	0.22	0.121	0.25
	Uncalibrated	0.175	0.24	0.530	0.27	0.616	0.27	0.079	0.22	0.109	0.26
	SDOF	0.028	0.32	0.136	0.31	0.174	0.32	0.012	0.32	0.017	0.32
B15	Full	0.068	0.39	0.521	0.39	0.743	0.39	0.079	0.39	0.100	0.39
	Calibrated	0.179	0.28	0.458	0.21	0.491	0.21	0.192	0.27	0.218	0.24
	Uncalibrated	0.178	0.29	0.490	0.18	0.525	0.19	0.191	0.27	0.214	0.25
	SDOF	0.038	0.38	0.183	0.27	0.223	0.27	0.044	0.38	0.053	0.38

In order to explore the possible improvement provided by a more complex reduced-order model, fragility analysis is performed also for a 4*Tav* model of B2. The results are reported in Table 4, where both the μ and the β values of the 4*Tav* are closer to the full model than the ones obtained by 1*Tav* for all limit-states. As expected, the transition from 1*Tav* to *nTav* improves the fragility curve reliability of the reduced-order model, especially for the more plan-asymmetric structures, at an obvious cost of higher complexity. Realizing even further gains deep into the nonlinear range may require adopting more elaborate schemes for determining the nonlinear properties of the 1*Tav*, 2*Tav* or *nTav* models[17].

Table 4 – μ and β values of fragility curves, accounting for all limit-states (IO, LS and NC), for the B2 building, comparing the full, the uncalibrated 1*Tav*, 4*Tav* and SDOF models for ductile and brittle failure modes.

Building	Model	IO		LS (Ductile)		NC (Ductile)		LS (Brittle)		NC (Brittle)	
		μ	β	μ	β	μ	β	μ	β	μ	β
B2	Full	0.090	0.29	0.446	0.29	0.596	0.29	0.057	0.30	0.098	0.29
	1*Tav*	0.200	0.29	0.512	0.22	0.550	0.22	0.137	0.29	0.207	0.29
	4*Tav*	0.126	0.28	0.505	0.24	0.581	0.24	0.111	0.28	0.188	0.28
	SDOF	0.028	0.32	0.161	0.33	0.232	0.33	0.017	0.32	0.031	0.32

Generally, three aspects can be observed: (a) there are no substantial differences among calibrated and uncalibrated fragility curves; (b) for the IO limit-state and the LS and NC ones evaluated involving brittle mechanisms, the reduced-order models return fair estimates of μ; (c) for the LS and NC limit-states involving ductile mechanisms, the reduced-order models provide conservative estimates of μ. In the end, of interest is the assessment of the overall behaviour of the entire sample, considering that one of the main purposes of the ideal/simplified models is to assess the class fragilities. Table 5 reports μ and β values for all buildings, limit-states and modelling approaches for the class. For ductile limit-states, percentage differences of μ are lower than 30%, while higher values are obtained for IO and brittle

limit-states. Regarding to β, percentage differences are in the order of 20-30% for all limit-states. Comprehensively, albeit with some imperfections, the proposed approach provides a satisfactory overall result of class fragility curves, especially if compared with results obtained via SDOF models, where percentage differences in terms of μ achieve values of 70%.

Table 5 – μ_C and β_C values of class fragility curves, accounting for all limit-states (IO, LS and NC), all modelling approaches (full, calibrated, uncalibrated and SDOF), all collapse mechanisms considered (ductile and brittle).

Model	IO		LS (Ductile)		NC (Ductile)		LS (Brittle)		NC (Brittle)	
	μ_C	β_C	μ_C	β_C	μ_C	β_C	μ_C	β_C	μ_C	β_C
Full	0.125	0.61	0.722	0.59	0.968	0.53	0.104	0.74	0.131	0.65
Calibrated	0.222	0.48	0.630	0.41	0.677	0.41	0.187	0.59	0.230	0.52
Uncalibrated	0.225	0.47	0.628	0.41	0.678	0.41	0.193	0.57	0.232	0.53
SDOF	0.039	0.53	0.218	0.60	0.280	0.51	0.032	0.60	0.048	0.72

7. CONCLUSIONS

A numerical procedure for eliciting simplified reduced-order models is presented, capable of predicting the seismic response of frame buildings characterized by plan irregularities. The tool proposes several rules and equations to reduce the degrees-of-freedom of buildings, starting from the near-full knowledge of geometrical and mechanical features, to obtain 3D reduced-order models composed of one or more one-by-one bay idealized structures, herein named tavolini. Despite reporting a certain loss of accuracy for the individual component failures, the procedure explores the possibility to reduce the computational cost in the global seismic assessment, especially for applications in class-level. The obtained results can be summarized as follows:

- The differences between calibrated and uncalibrated versions of 3D reduced-order models show that the calibration is not strictly necessary.
- Comparing small cloud analyses on full models and IDAs on 3D reduced-order ones, the results of the structural analysis show a certain agreement between the two approaches, highlighting that with an appropriate choice of IM and EDP values, this simplified approach can offer favourable compromises of computational cost versus assessment accuracy.
- Comparing fragility curves for a number of buildings at different limit-states, the results show similar estimates at low-EDP capacity values (e.g., brittle failures) and some differences for high-EDP ones (e.g., ductile mechanisms). Actually, in the context of building-level assessment, it is not possible to establish a generalizable trend, especially for safety limit-states with ductile mechanisms. On the other hand, 3D reduced-order models can ensure a reliable estimate for purposes of class-level seismic assessment, with a good coverage of the full modelling space;

In the end, despite its limitations, the proposed order-reduction may not be optimal for building-specific investigations but can offer solutions for class-level assessment, realizing a good compromise between the high-accuracy/low-coverage of few MDOF archetypes versus the low-accuracy/high-coverage of many generic SDOF models. Further developments could provide some upgrades of tavolino model, as for example by introducing new rules for better accounting the nonlinear properties of the original building (e.g., a weighted average of the inelastic properties by beams or columns lengths[32]) and introducing shear failures and non-structural elements in modelling.

ACKNOWLEDGEMENTS

The first and the last authors acknowledge funding by the Italian Department of Civil Protection in the framework of the national project DPC-ReLUIS 2019-2021. Additional financial support has been provided by the Eugenides Foundation in Greece (scholarship for doctoral studies in NTUA grant) and by the European Commission through the Horizon 2020 program "HYPERION–Development of a decision support system for improved resilience & sustainable reconstruction of historic areas to cope with climate change & extreme events based on novel sensors and modelling tools", Grant Agreement No. 821054.

REFERENCES

1. Silva V., Akkar S., Baker J.W., Bazzurro P., Castro J.M., Crowley H., Dolsek M., Galasso C., Lagomarsino S., Monteiro R., Perrone D., Pitilakis K., Vamvatsikos D. Current challenges and future trends in analytical fragility and vulnerability modelling. Earthquake Spectra, 2019, 35(4). DOI: 10.1193/042418EQS101O
2. Silva. V., Crowley H., Varum H., Pinho R., Sousa L. Investigation of the characteristics of Portuguese regular moment-frame RC buildings and development of a vulnerability model. Bulletin of Earthquake Engineering, 2014, 13: 1455-1490. DOI: 10.1007/s10518-014-9669-y
3. Sousa L, Silva V, Marques M, Crowley H. On the treatment of uncertainties in the development of fragility functions for earthquake loss estimation of building portfolios. Earthquake Engineering & Structural Dynamics, 2016, 45(12), 1955–1976. DOI:10.1002/eqe.2734
4. Ruggieri S., Porco F., Uva G., Vamvatsikos D. Two frugal options to assess class fragility and seismic safety for low-rise reinforced concrete school buildings in Southern Italy. Bulletin of Earthquake Engineering, 2021, 19: 1415-1439. DOI: 10.1007/s10518-020-01033-5
5. Baltzopoulos G., Baraschino R., Iervolino I. On the number of records for structural risk estimation in PBEE. Earthquake Engineering and Structural Dynamics, 2018, 48(5): 489-506. DOI: 10.1002/eqe.3145
6. Sousa L., Silva V., Marques M., Crowley H. On the treatment of uncertainties in the development of fragility functions for earthquake loss estimation of building portfolios. Earthquake Engineering and Structural Dynamics, 2016, 45(12): 1955-1976. DOI: 10.1002/eqe.2734
7. Ruggieri S., Perrone D., Leone M., Uva G., Aiello M.A. A prioritization RVS methodology for the seismic risk assessment of RC school buildings. International Journal of Disaster Risk Reduction, 2020, 54, 101807. DOI: 10.1016/j.ijdrr.2020.101807
8. Saiidi M., Sozen M.A. Simple nonlinear seismic analysis of RC structures. Journal of the Structural Division-ASCE., 1981, 107(5): 937-952. DOI: 10.1061/JSDEAG.0005714
9. Fajfar P., Gaspersic P. The N2 method for the seismic damage analysis of RC buildings. Earthquake Engineering and Structural Dynamics, 1996, 25(1): 31−46. DOI: 10.1002/(SICI)1096-9845(199601)25:1<31::AID-EQE534>3.0.CO;2-V
10. Bakalis K., Fragiadakis M., Vamvatsikos D. Surrogate modeling for the seismic performance assessment of liquid storage tanks. Journal of Structural Engineering, 2017, 143(4): 4016199. DOI: 10.1061/(ASCE)ST.1943-541X.0001667
11. Nakashima M., Ogawa K., Inoue K. Generic frame model for simulation of earthquake responses of steel moment frames. Earthquake Engineering and Structural Dynamics, 2002, 31(3):671– 692. DOI: 10.1002/eqe.148
12. Ogawa K., Kamura H., Inoue K. Modeling of the moment resistant frame to fishbone-shaped frame for the response analysis. Journal of Structural and Construction Engineering (Transactions of AIJ), 1999, 64(521): 119-126. DOI: 10.3130/aijs.64.119_3
13. Luco N., Mori Y., Funahashi Y., Cornell C.A., Nakashima M. Evaluation of predictors of nonlinear seismic demands using 'fishbone' models of SMRF buildings. Earthquake Engineering and Structural Dynamics, 2003, 32(14): 2267–2288. DOI: 10.1002/eqe.331
14. Mori Y., Yamanaka T., Luco N., Nakashima M., Cornell C.A. Predictors of seismic demand of SMRF buildings considering post-elastic mode shape. 13th World Conference on Earthquake Engineering, 2004, Vancouver, Canada.
15. Mori Y., Yamanaka T., Luco N., Cornell C.A. A static predictor of seismic demand on frames based on a post-elastic deflected shape. Earthquake Engineering and Structural Dynamics, 2006, 35(10): 1295–1318. DOI: 10.1002/eqe.587
16. Khaloo A.R., Khosravi H. Modified fish-bone model: A simplified MDOF model for simulation of seismic responses of moment resisting frames. Soil Dynamics and Earthquake Engineering, 2013, 55: 195-210. DOI: 10.1016/j.soildyn.2013.09.013
17. Jamšek A., Dolšek M. Seismic analysis of older and contemporary reinforced concrete frames with the improved fish-bone model. Engineering Structures, 2020, 212, 110514. DOI: 10.1016/j.engstruct.2020.110514

18. Gidaris I., Taflanidis A.A. Parsimonious modeling of hysteretic structural response in earthquake engineering: calibration/validation and implementation in probabilistic risk assessment. Engineering Structures, 2013, 49: 1017–1033. DOI: 10.1016/j.engstruct.2012.12.030
19. Patsialis D., Taflanidis A.A. Reduced-order modeling of hysteretic structural response and applications to seismic risk assessment. Engineering Structures, 2020, 209, 110135. DOI: 10.1016/j.engstruct.2019.110135
20. Bovo M., Savoia M. Evaluation of seismic response of buildings using dynamic analysis on stick models. COMPDYN 2015. 5th ECCOMAS Thematic Conference on Computational Methods in Structural Dynamics and Earthquake Engineering. M. Papadrakakis. V. Papadopoulos. V. Plevris (eds.) Crete Island. Greece. 25–27 May 2015
21. d'Aragona M.G., Polese M., Prota A. Stick-IT: A simplified model for rapid estimation of IDR and PFA for existing low-rise symmetric infilled RC building typologies. Engineering Structures, 2020, 223, 111182. DOI: 10.1016/j.engstruct.2020.111182
22. d'Aragona, M.G., Polese M., Di Ludovico M., Prota A. The use of Stick-IT model for the prediction of direct economic losses. Earthquake Engineering and Structural Dynamics, 2021. DOI: 10.1002/eqe.3429
23. Blasone V, Basaglia A, De Risi R, De Luca F, Spacone E. A simplified model for seismic safety assessment of reinforced concrete buildings: framework and application to a 3-storey plan-irregular moment resisting frame. Engineering Structures 2022; 250: 113348. DOI: 10.1016/j.engstruct.2021.113348.
24. Lachanas C, Vamvatsikos D Model type effects on the estimated seismic response of a 20-story steel moment resisting frame. Journal of Structural Engineering, 2020, https://doi.org/10.1061/(ASCE)ST.1943-541X.0003010.
25. Tsompanakis Y., Lagaros N.D., Stavroulakis G.E. (2008). Soft computing techniques in parameter identification and probabilistic seismic analysis of structures. Advances in Engineering Software, 39(7): 612-624. DOI: 10.1016/j.advengsoft.2007.06.004
26. Taflanidis A.A., Jia G., Gidaris I. Natural Hazard Probabilistic Risk Assessment Through Surrogate Modeling. Multi-hazard Approaches to Civil Infrastructure Engineering, P. Gardoni. J.M. LaFave (eds.), 2013, DOI 10.1007/978-3-319-29713-2_4
27. Lagaros N.D., Fragiadakis M. Fragility assessment of steel frames using neural networks. Earthquake Spectra, 2007, 23(4): 735–752. DOI: 10.1193/1.2798241
28. Gavin H.P., Yau S.C. High-order limit-state functions in the response surface method for structural reliability analysis. Structural Safety, 2008, 30(2): 162-179. DOI: 10.1016/j.strusafe.2006.10.003
29. Taflanidis A.A., Cheung S.H. Stochastic sampling using moving least squares response surface approximations. Probabilistic Engineering Mechanic, 2012, 28: 216-224. DOI: 10.1016/j.probengmech.2011.07.003
30. Gidaris I., Taflanidis A.A., Mavroeidis G.P. Kriging metamodeling in seismic risk assessment based on stochastic ground motion. Earthquake Engineering and Structural Dynamics, 2015, 44(14): 2377-2399 DOI: 10.1002/eqe.2586
31. Gidaris I., Taflanidis A.A. Optimal Design of Floor Isolation Systems subject to Multiple Reliability Criteria utilizing Kriging Surrogate Modeling. in Y. Tsompanakis. J. Kruis. B.H.V. Topping. (Editors). Proceedings of the Fourth International Conference on Soft Computing Technology in Civil. Structural and Environmental Engineering. Civil-Comp Press. Stirlingshire, 2015, UK. Paper 25. doi:10.4203/ccp.109.25
32. Priestley MJN, Calvi GM, Kowalsky MJ. Displacement-Based Seismic Design of Structures. Pavia, Italy: IUSS Press; 2007.
33. CEN Eurocode 8: Design of structures for earthquake resistance - Part 3: Assessment and Retrofitting of Buildings, EN 1998, European Committee for Standardisation, Brussels, 2004.
34. O'Reilly G.J., Sullivan T.J. Modeling Techniques for the Seismic Assessment of the Existing Italian RC Frame Structures. Journal of Earthquake Engineering, 2017, 23(8): 1–35. DOI: 10.1080/13632469.2017.1360224.
35. Computer and Structures. SAP2000. Advanced 18 Structural Analysis Program –Manual. Computer and Structures. Inc. Berkeley, 2016, California, USA.
36. McKenna F. OpenSees: a framework for earthquake engineering simulation. Computing in Science and Engineering, 2011, 13(4): 58–66. DOI: 10.1109/MCSE.2011.66

37. Jalayer F, Franchin P, Pinto PE. A scalar damage measure for seismic reliability analysis of RC frames. Earthquake Engineering & Structural Dynamics, 2007, 36(13): 2059–2079. DOI: 10.1002/eqe.704
38. Galanis PH, Moehle JP. Development of collapse indicators for risk assessment of older-type reinforced concrete buildings. Earthquake Spectra, 2015, 31(4): 1991-2006. DOI:10.1193/08061 3EQS2 25M
39. Ricci P., Manfredi V., Noto F., Terrenzi M., Petrone C., Celano F., De Risi M.T., Camata G., Franchin P., Magliulo G., Masi A., Mollaioli F., Spacone E., Verderame G.M. Modeling and Seismic Response Analysis of Italian Code-Conforming Reinforced Concrete Buildings. Journal of Earthquake Engineering, 2018, 22: 105-139. DOI: 10.1080/13632469.2018.1527733
40. Kohrangi M., Vamvatsikos D. INNOSEIS ground motion set for medium seismicity European sites, 2016. URL http://innoseis.ntua.gr/medium_record_set.rar.
41. Lin T., Haselton C.B., Baker J.W. Conditional spectrum-based ground motion selection. Part I: hazard consistency for risk-based assessments. Earthquake engineering and structural dynamics, 2013, 42(12): 1847-1865. DOI: 10.1002/eqe.2301
42. Kohrangi M., Vamvatsikos D., Bazzurro P. Site dependence and record selection schemes for building fragility and regional loss assessment. Earthquake Engineering and Structural Dynamics, 2017, 46(10): 1625–1643. DOI: 10.1002/eqe.2873
43. ASCE 7-16. Minimum Design Loads for Buildings and Other Structures. Commentary. American Society of Civil Engineers, 2017, doi:10.1061/9780784412916
44. Kazantzi A.K., Vamvatsikos. D. Intensity measure selection for vulnerability studies of building classes. Earthquake engineering and structural dynamics,2015, 44(15): 2057-2073. DOI: 10.1002/eqe.2603
45. Vamvatsikos D., Cornell C.A. Applied incremental dynamic analysis. Earthquake Spectra, 2004, 20(2): 523–553. DOI: 10.1193/1.1737737
46. Cornell C.A., Jalayer F., Hamburger R.O., Foutch D. Probabilistic Basis for 2000 SAC Federal Emergency Management Agency Steel Moment Frame Guidelines. Journal of Structural Engineering, 2002, 128(4). DOI: 10.1061/(ASCE)0733-9445(2002)128:4(526)
47. Jalayer F., Cornell C.A. Alternative non-linear demand estimation methods for probability-based seismic assessments. Earthquake Engineering and Structural Dynamics, 2009, 38(8): 951–972. DOI: 10.1002/eqe.876
48. Bakalis K, Vamvatsikos D. Seismic Fragility Functions via Nonlinear Response History Analysis. Journal of Structural Engineering, 2018, 144(10). DOI: 10.1061/(ASCE)ST.1943-541X.0002141
49. Zareian, F., Ibarra, L., and Krawinkler, H. Seismic demands and capacities of single-story and low- rise multi-story woodframe structures. Proceedings of the 13th World Conference on Earthquake Engineering, 2004, Vancouver, B.C., Canada.
50. FEMA. Quantification of Building Seismic Performance Factors. FEMA P-695. prepared by Applied Technology Council for Federal Emergency Management Agency, 2009, Washington, D.C.
51. Gentile R., Galasso C. Simplicity versus accuracy trade-off in estimating seismic fragility of existing reinforced concrete buildings. Soil Dynamics and Earthquake Engineering, 2021, 144, 106678. DOI: https://doi.org/10.1016/j.soildyn.2021.106678